基于LP$_{01}$和LP$_{11}$模式共存的单光纤光镊实现生物细胞多路捕获和操纵

陈朋，党雨婷，钟慧，姜春雷*

东北石油大学电气信息工程学院，黑龙江 大庆 163318

摘要 提出了一种用于生物细胞多路捕获与操纵的单光纤光镊。基于两种不同模式的光纤错位拼接，实现了LP$_{01}$和LP$_{11}$模式共存。该光镊的输出光场具有多个聚焦光斑，能够在多个支路上同时捕获和操纵多个生物细胞。仿真和实验结果表明，该光镊能够在三个支路上同时捕获和操纵多个小球藻细胞，在光镊移动速度约为 14 μm/s 时仍能保持捕获稳定。该光镊结构简单，为生物传感和直接检测生物信号提供了更多可能。

关键词 光纤光学；光纤光镊；LP$_{01}$模式和LP$_{11}$模式；多路捕获和操纵；生物传感

中图分类号 Q631　　**文献标志码** A　　　　　　**DOI:** 10.3788/AOS221560

1 引　　言

目前，一些生物光子器件或细胞间相互作用和通信中需要捕获微粒，尤其是捕获多个微粒。自 1986 年 Ashkin 等[1]发明光镊以来，光镊已成为一种重要的工具，被广泛应用于细胞、病毒、原子、胶体等微粒的操作和研究中[2-9]。在传统光镊的基础上，研究人员利用全息束整形技术[9-11]或干涉测量技术[12-13]将多个粒子捕获到结构光场中，并采用全息光镊[10, 14-15]、螺旋相位前单光束[16]、光结合[17]等多种方法实现了多粒子的多向排列。然而，以上这些技术需要庞大的光学元件，从而使得光镊系统变得复杂，阻碍了操作的灵活性。光纤因其结构紧凑、便于集成、操作灵活和适用范围广等优点，成为了广泛应用于光学捕获和光学操纵的工具[18-21]。

为了克服传统光镊捕获多个微粒的不足，研究人员利用光纤光镊来捕获多个微粒。2009 年，Liu 等[22]使用倾斜的双光纤光镊装置构建了多个光阱，实现了在二维和三维上对多个微粒的捕获。2013 年，Barron 等[23]利用多芯光纤对多个粒子和大肠杆菌细胞进行二维光学干涉捕获。还有科研人员利用光纤阱[24]和光热效应[25]对大量微粒进行操控。2017 年，Li 等[26-27]不仅利用单光纤实现了对多个微粒的捕获，还利用错位的两个单模光纤实现了多个细胞的操控、偏转和拉伸[28]。2018 年，Velázquez-Benítez 等[29]利用光子晶体模式复用技术操控多个微粒，粒子的旋转既可以通过线偏振（LP）模式的切换实现，也可以通过输入光的偏振旋转实现。Zhang 等[30-33]利用LP$_{11}$模式实现了对多个微粒的捕获、偏转等。以上方法大多利用多个光纤实现对多个微粒的操纵，但基于多芯光纤和光子晶体的光纤探针存在结构复杂、复制困难等缺陷。

针对多芯光纤和光子晶体光纤探针结构复杂的问题，提出了两种模式复合的单光纤光镊结构。该结构将两种不同模式的光纤错位拼接，使输出光场中LP$_{01}$和LP$_{11}$模式共存。由于在光纤中激发LP$_{11}$模式光束的同时，LP$_{01}$模式光束也会被激发，但两种模式光束具有不同的传播常数，即会表现出不同的聚焦光场，故能够实现多个生物细胞的多路捕获与排列。利用不同模式光束具有不同的聚焦光场，实现了在不同方向捕获多个小球藻细胞。然后，被捕获的小球藻细胞被作为透镜对光束进行再次聚焦以捕获下一个细胞，从而形成多个生物链条。该光纤光镊结构简单、成本低，为生物传感和直接检测生物信号提供了更多可能。

2 原理与数值模拟

光纤中存在多种模式，光纤中传播的模式数量取决于传输光波在光纤中的归一化频率参数 V[32]。归一化频率参数 V 由入射激光波长 λ、纤芯的半径 α、纤芯折射率 n_{core} 和包层折射率 $n_{cladding}$ 决定，即

$$V = \frac{2\pi a}{\lambda} \sqrt{n_{\mathrm{core}}^2 - n_{\mathrm{cladding}}^2}。 \qquad (1)$$

当 $V < 2.405$ 时，光波在光纤中激发的模式为 LP_{01} 模式。当 $2.405 \leqslant V \leqslant 3.832$ 时，光波在光纤中激发的模式为 LP_{11} 模式。当 $V > 3.832$ 时，光波在光纤中将会激发更高阶的模式。

对于常见的 980 nm 单模光纤（SMF），$V = 2.2243 < 2.405$ 不能满足 LP_{01} 和 LP_{11} 模式共存。对于常见的 1550 nm SMF，$V = 2.2638 < 2.405$ 也不能满足 LP_{01} 和 LP_{11} 模式共存。如果要实现 LP_{01} 和 LP_{11} 模式共存，可以将 980 nm SMF 与 1550 nm SMF 拼接起来，将 980 nm SMF 与 980 nm 激光光源连接，再将

1550 nm SMF 作为输出端。对于 1550 nm SMF，纤芯折射率为 $n_{\mathrm{core}} = 1.4626$，包层折射率为 $n_{\mathrm{cladding}} = 1.45732$，纤芯半径为 $a = 4.5$ μm，根据式（1），当输入激光为 980 nm 光源（$\lambda = 980$ nm）时，可得到 $2.405 < V = 3.5824 < 3.832$。因此，光波在光纤中激发出 LP_{11} 模式光束的同时，LP_{01} 模式光束也会被激发。如果将 980 nm SMF 与 1550 nm SMF 共轴拼接，在 1550 nm SMF 输出端处光波能量主要分布在 LP_{01} 模式中，如图 1(a)所示。为了在 LP_{11} 模式下获得具有更高能量比的光波，需要在 980 nm SMF 和 1550 nm SMF 之间进行较小的横向芯偏移，如图 1(b)所示。
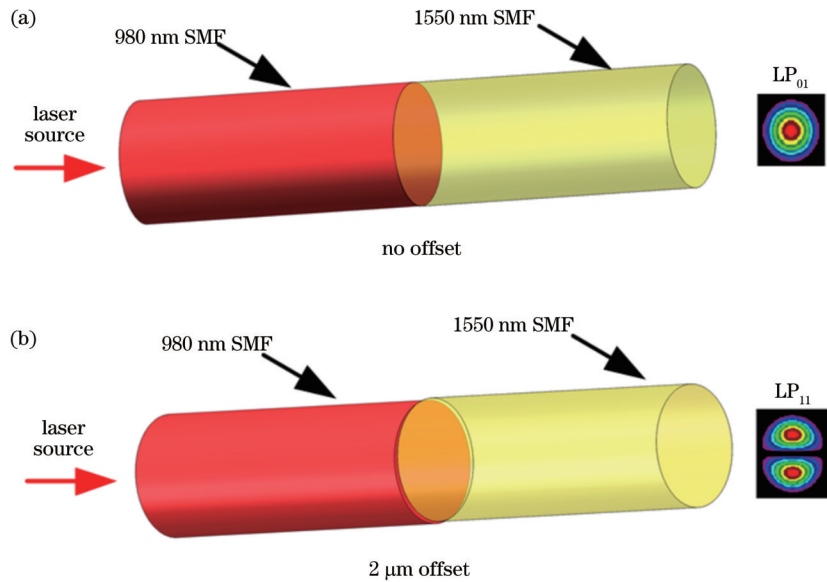

图 1　光纤拼接示意图。(a) 980 nm SMF 与 1550 nm SMF 共轴拼接；(b)横向芯偏移 2 μm 后的 980 nm SMF 和 1550 nm SMF 拼接
Fig. 1　Schematic diagram of fiber splicing. (a) Coaxial splicing of 980 nm SMF and 1550 nm SMF; (b) splicing of 980 nm SMF and 1550 nm SMF with 2 μm transverse core offset

为了确定横向偏移量，实验记录了两根光纤的错位量与 1550 nm 标准单模光纤中的光功率值，绘制出的曲线如图 2 所示。可以看出，当两根光纤的拼接错位量逐渐增大时，光功率逐渐衰减直至零。当错位量在 0～2 μm 区间内时，LP_{01} 与 LP_{11} 模式光束的功率衰减得较小，故需要将错位量控制在 0～2 μm 区间内。当选择横向偏移量为 2 μm 时，既有足够大的光功率可以满足光镊的捕获需求，又可以达到 LP_{01} 与 LP_{11} 聚焦光场能量相当的条件。

为了实现在不同方向上进行多微粒捕获和操纵，还需要使出射光场具有较小的束腰和较大的梯度分布。因此，需要将 1550 nm SMF 的输出端拉成锥形，实验中使用火焰加热和拉伸技术对商业单模光纤（康宁公司，连接器类型为 FC/PC，芯径为 9 μm，包层直径为 125 μm）进行加工实现。首先，使用光纤剥离器将光纤的缓冲层和聚合物夹层剥离，得到直径为 125 μm、长度为 3 cm 的裸纤。为了防止光纤断裂和翘
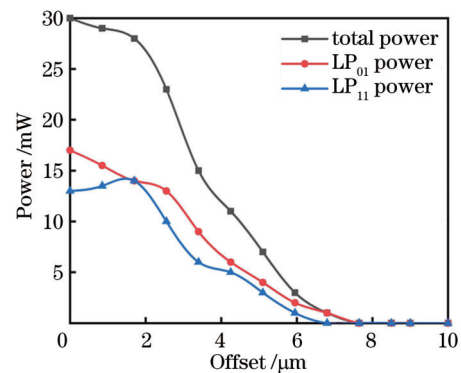

图 2　光纤拼接错位量曲线
Fig. 2　Fiber splicing offset curve

起，采用玻璃毛细管包覆。毛细管外的裸露光纤用酒精灯的外火焰（温度大约为 500 ℃）加热 40 s，直至光纤的熔点，拉伸速度大约为 1 mm/s，光纤在 1 cm 的长度范围内逐渐变细，直径由 125 μm 减小到 10 μm。然后，以 10 mm/s 左右的速度快速拉断光纤，形成锥形尖

端。光纤尖端的末端是由熔融光纤的表面张力形成的。最后,用一块酒精棉仔细擦拭锥形纤维的超细尖端,如图3所示。距离光纤尖端5.7 μm处的角度为 $\theta_1=58°$,锥形光纤尖端的锥角为 $\theta_2=43°$。该方法制备的带有尖端的锥形光纤的重复性好,可以制备形状和尺寸相近的不同锥形光纤。
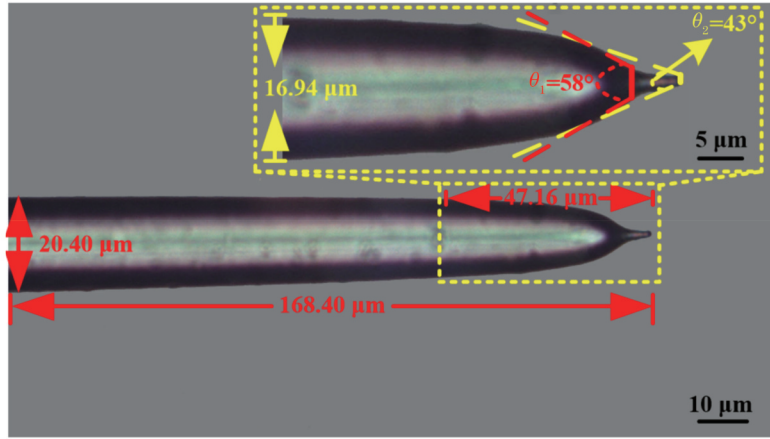

图 3　拉伸的光纤尖端在光学显微镜下的图像

Fig. 3　Image of stretched fiber tip under optical microscope

单个模式的光纤光镊因模式数量的限制,可实现的操作功能单一,很难实现多个微粒的捕获,更不用说从多个支路进行同时捕获。由于不同模式光场经一根光纤探针输出后形成的稳定捕获点不同,故两种模式共存的单光纤光镊可以很容易实现多路同时捕获多个微粒。

为了分析复合模式光纤的聚焦光场特性,利用仿真软件中的电磁波频域模块,基于有限元分析方法建立了二维模型,模拟了 LP_{01} 和 LP_{11} 模式光束的输出光场分布,并计算了施加在小球藻细胞上的光辐射压力。仿真条件:激光光源波长为980 nm;使用980 nm SMF 和 1550 nm SMF 错位拼接(错位 2 μm)的复合光纤;1550 nm SMF 作为输出端,其输出端的尖端锥角为 43°,纤芯折射率和周围介质(水)的折射率分别为1.4626和1.33;选取小球藻细胞作为被捕获的微粒,其折射率为1.45[34],直径约为3 μm;输出端激光功率为10 mW。软件基于有限元法计算捕获力,故目标粒子的捕获力 F[35] 可以表示为

$$F=\oint_S (\langle T_{\mathrm{M}}\rangle \cdot \boldsymbol{n})\mathrm{d}S, \qquad (2)$$

式中: S 为目标粒子周围的封闭表面; $\boldsymbol{n}$ 为向外垂直于 S 的单位向量; $\langle T_{\mathrm{M}}\rangle$ 为时间平均麦克斯韦压力张量,其表达式为

$$\langle T_{\mathrm{M}}\rangle=\frac{1}{2}\mathrm{Re}\Bigg[-\frac{1}{2}\Big(\varepsilon|\boldsymbol{E}|^2+\mu|\boldsymbol{H}|^2\Big)\boldsymbol{I}+$$
$$\varepsilon\boldsymbol{E}\boldsymbol{E}^*+\mu\boldsymbol{H}\boldsymbol{H}^*\Bigg], \qquad (3)$$

式中: $\boldsymbol{I}$ 为单位并矢; ε 为介电常数; μ 为磁导率; $\boldsymbol{E}$ 和 $\boldsymbol{E}^*$ 为电场; $\boldsymbol{H}$ 和 $\boldsymbol{H}^*$ 为磁场。图4(a)、(b)分别显示了光纤探针附近 LP_{01} 和 LP_{11} 模式光束的输出光场分布。图4(a)表明 LP_{01} 模式光束集中在光纤探针尖端

处,产生了一个光斑。图4(b)表明 LP_{11} 模式光束主要分布在光纤探针的两侧,产生了两个小光斑。 LP_{01} 模式光束在光纤探针尖端聚焦,表明小球藻细胞会被捕获在光纤尖端处。 LP_{11} 模式光束的会聚位置在光纤尖端两侧,光场梯度分布较大,故光纤尖端外部的小球藻细胞会被吸引并向光纤尖端移动。图4(c)显示了 LP_{01} 和 LP_{11} 模式光束共存的光场分布,可以明显看出此时的光场同时具有 LP_{01} 和 LP_{11} 模式光束的特性。在光纤中激发 LP_{11} 模式光束的同时, LP_{01} 模式光束也存在,由于两种模式光束具有不同的传播常数,故会表现出不同的聚焦光场。也就是说, LP_{01} 模式与 LP_{11} 模式通过相同的光纤探针后产生的稳定捕获点不同。

当 LP_{01} 与 LP_{11} 两种模式共存时, LP_{01} 光场内施加在小球藻细胞上的轴向捕获力和横向捕获力如图5(a)、(b)所示。由图5(a)可知:在 x 轴 46.00~47.70 μm 范围内,轴向力大于零,这意味着小球藻细胞沿着光束的传播方向移动,远离光纤尖端;在 x 轴 47.70~48.25 μm 范围内,轴向力小于零,这意味着小球藻沿着光束传播的反方向移动,靠近光纤尖端。因此,小球藻细胞被稳定地困在 $x=47.70$ μm、轴向力为零的轴向位置处。然后,计算在 $x=47.70$ μm 轴向位置处施加在小球藻细胞上的横向力。由于光场沿 x 轴对称,可以在 x 轴上捕获粒子,故粒子受到的横向捕获力是中心对称的,如图5(b)所示。当施加在小球藻细胞上的轴向捕获力和横向捕获力为零时,粒子保持平衡。

LP_{11} 光场内施加在光纤尖端两侧小球藻细胞上的轴向捕获力和横向捕获力如图5(c)、(d)所示。由图5(c)可知,小球藻细胞可以稳定地被困在 $x=44.48$ μm 位置处,该位置的横向捕获力如图5(d)所示。当小球
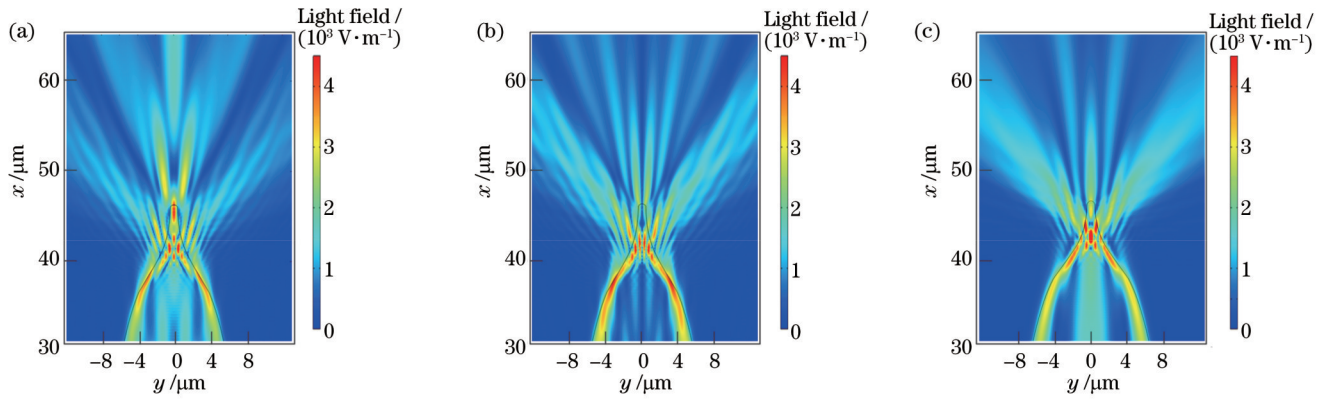
图 4 不同模式光束光场分布。(a) LP$_{01}$模式;(b) LP$_{11}$模式;(c) LP$_{01}$和 LP$_{11}$模式

Fig. 4 Light field distributions of different mode beams. (a) LP$_{01}$ mode; (b) LP$_{11}$ mode; (c) LP$_{01}$ and LP$_{11}$ modes
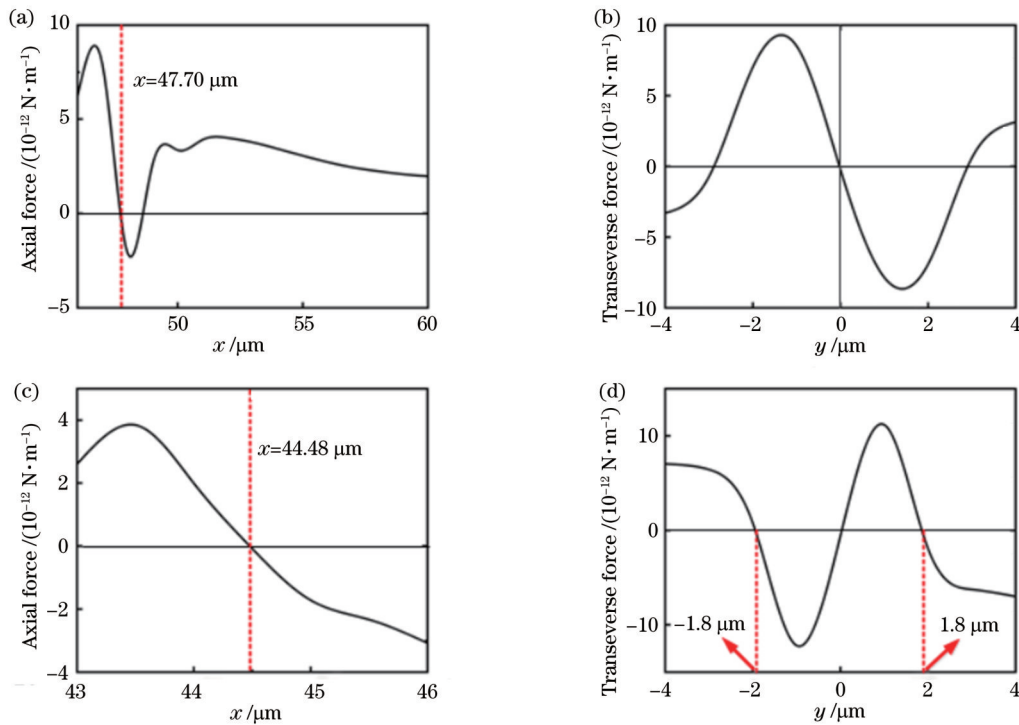

图 5 两种模式共存时作用在小球藻细胞上的捕获力模拟结果(光纤的出射方向为+x轴)。(a)沿 x 轴作用在小球藻细胞上的轴向力;(b) $x=47.70$ μm 位置处小球藻细胞受到的横向力;(c)沿 $y=-1.8$ μm 作用在小球藻细胞上的轴向力;(d) $x=44.48$ μm 位置处小球藻细胞受到的横向力

Fig. 5 Simulation results of capture force acting on *Chlorella* cells when two modes coexist (outgoing direction of fiber is +x axis). (a) Axial force acting on *Chlorella* cells along x-axis; (b) transeverse force acting on *Chlorella* cells at $x=47.70$ μm; (c) axial force acting on *Chlorella* cells along $y=-1.8$ μm; (d) transeverse force acting on *Chlorella* cells at $x=44.48$ μm

藻细胞偏离+y沿着−1.8 μm 方向时,粒子将受到向下的拉力,将其拉回 y 等于−1.8 μm 的轴上。当小球藻细胞偏离−y沿着−1.8 μm 方向时,粒子将受到一个向上的拉力,将它拉回 y 等于−1.8 μm 的轴上。因此,小球藻细胞被捕获在 $(x, y) = (44.48$ μm,−1.8 μm)位置处。在横向上,光场沿轴向也是对称的,作用在粒子上的力表现为中心对称,故小球藻细胞的另外一个被捕获位置为 $(x, y) = (44.48$ μm,1.8 μm)。

3 实验结果与讨论

3.1 实验装置

为了验证仿真分析的有效性,搭建了图 6 所示的实验装置。波长为 980 nm 的激光器(宁波烨博光电科技有限公司,YA605)作为光源,输出功率为 0~25 mW。考虑到功率的大小对于颗粒稳定性捕获的重要性,实验中保证光纤端输出功率为 10 mW 左右。采用 980 nm SMF 和 1550 nm SMF 错位 2 μm 拼接的复

合光纤,其中 980 nm SMF 作为输入端与激光光源连接,1550 nm SMF 作为输出端浸入小球藻细胞溶液中。光纤探针由毛细管包裹,且固定在三维操作台上。将载玻片安装在 xyz 手动平移台上以确保定位的精确性和稳定性。所用生物细胞为小球藻细胞,折射率为1.45。将含有小球藻细胞的溶液放置在盖玻片与载玻片之间,并且中间留有 2~3 mm 的距离形成腔室,以减弱微粒在溶液中的布朗运动,允许小球藻细胞长时间工作在一个稳定的环境下。然后,将带电荷耦合器件(CCD)相机的界面显微镜与带 CCD 相机的个人计算机(PC)相连,以记录实验图像。
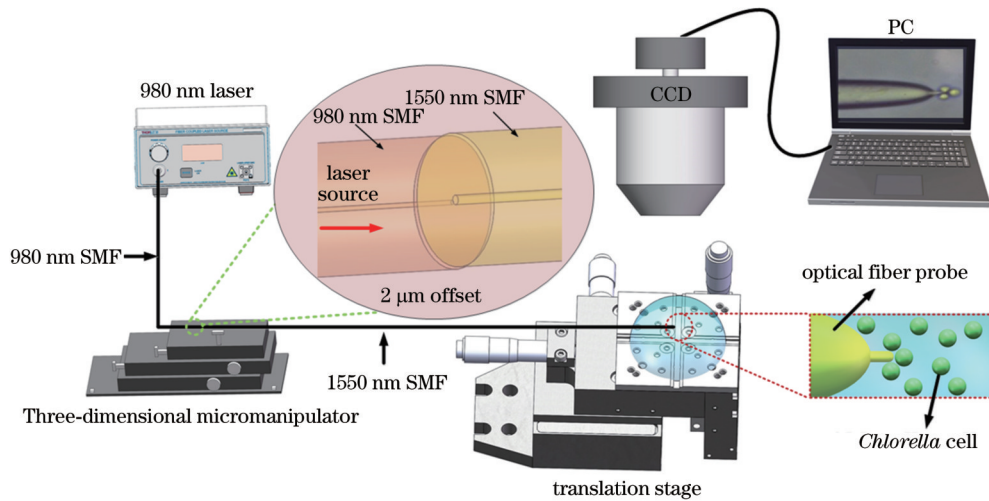

图 6   实验装置图
Fig. 6   Diagram of experimental setup

3.2   结果与讨论

当 980 nm 激光打开时,光纤探针有效陷阱区域内的小球藻细胞被吸引到光纤尖端路径 1 处,如图 7(a)左侧的图所示。此时,光纤尖端处的小球藻细胞被稳定捕获。该小球藻细胞相当于一个透镜,聚焦光束后产生一个新的有效陷阱。如图 7(a)中间的图所示,有效区域内的小球藻细胞会沿着路径 1 移动到第二个小球藻处,然后被稳定捕获。同样地,第三个小球藻细胞沿着路径 1 被捕获,如图 7(a)右侧的图所示。LP_{11} 模束的会聚位置在光纤尖端两侧,光场梯度分布较大,故光纤尖端外部的小球藻细胞会被吸引并向光纤尖端两侧(路径 2 和路径 3)移动,如图 7(b)所示。

图 7   在 LP_{01} 和 LP_{11} 模式共存的光束下,不同方向多生物细胞(小球藻细胞)的捕获。(a)小球藻细胞沿着路径 1 被捕获;(b)小球藻细胞被吸引到光纤尖端两侧(路径 2 和路径 3)
Fig. 7   Capture of multibiotic cells (*Chlorella* cells) in different directions under coexisting beams of LP_{01} and LP_{11} modes. (a) *Chlorella* cells captured along path 1; (b) *Chlorella* cells attracted to both sides of fiber tip (path 2 and path 3)

为了验证小球藻细胞被捕获的稳定性,所形成的颗粒链或细胞链可以在三维空间中实现轴向约束和长范围的柔性传递[36],对光纤进行了移动,如图 8 所示。当时间 t 在 0~11 s 范围内,光纤向右缓慢移动时,小球藻细胞也随着光纤缓慢移动到相应位置。当 t 在 11~16 s 范围内时,小球藻细胞随着光纤上下移动。当 t 在 16~26 s 范围内时,光纤向左缓慢移动,小球藻细胞随着光纤缓慢移动到相应位置处。光纤沿着与之前相反的方向移动一定距离,酵母菌细胞同样随着光纤移动相同距离。

图 8 小球藻细胞随光纤移动过程的实验图
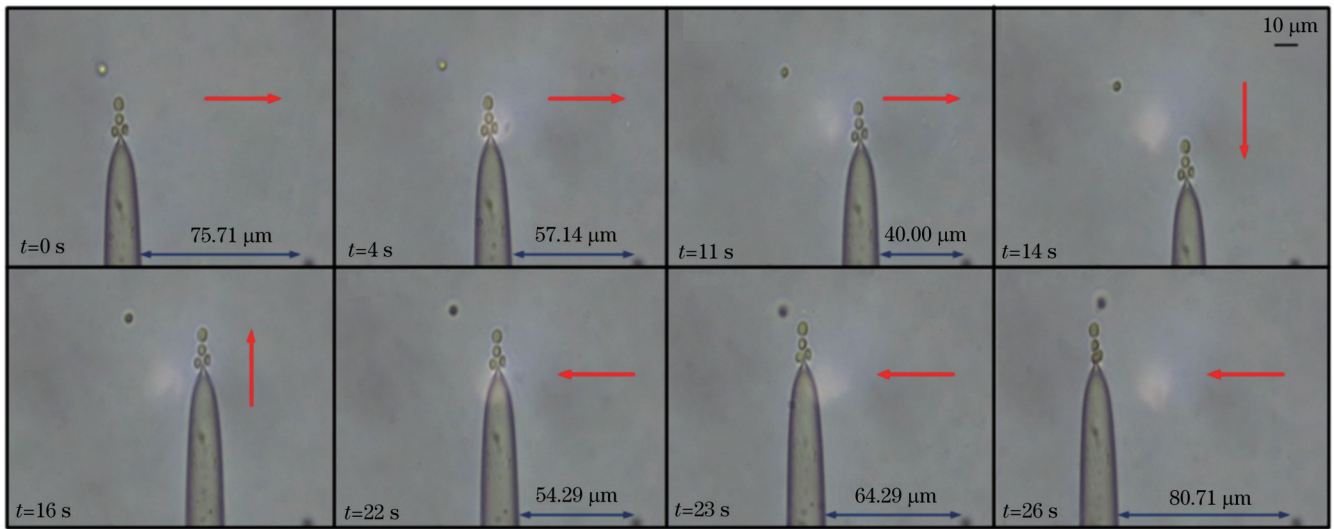
Fig. 8 Experimental diagram of movement process of *Chlorella* cells with optical fiber

接下来,为了更好地描述光纤光镊捕获小球藻细胞的能力,研究了小球藻细胞位移和时间的关系,如图9所示。可以看出:在0~11 s时间范围内,小球藻细胞随着光纤向右移动,此时小球藻细胞随光纤运动的速度约为4 μm/s;在11~16 s时间范围内,小球藻细胞随着光纤上下移动,此时小球藻细胞随光纤运动的速度分别约为14 μm/s和10 μm/s;在16~26 s时间范围

内,小球藻细胞随着光纤向左移动,此时小球藻细胞随光纤运动的速度约为5.5 μm/s。

实验过程表明,该光纤光镊能够实现在三个路径上同时捕获和操纵多个小球藻细胞,与仿真分析结果一致,且在0~14 μm/s的移动速度条件下捕获稳定性很好。
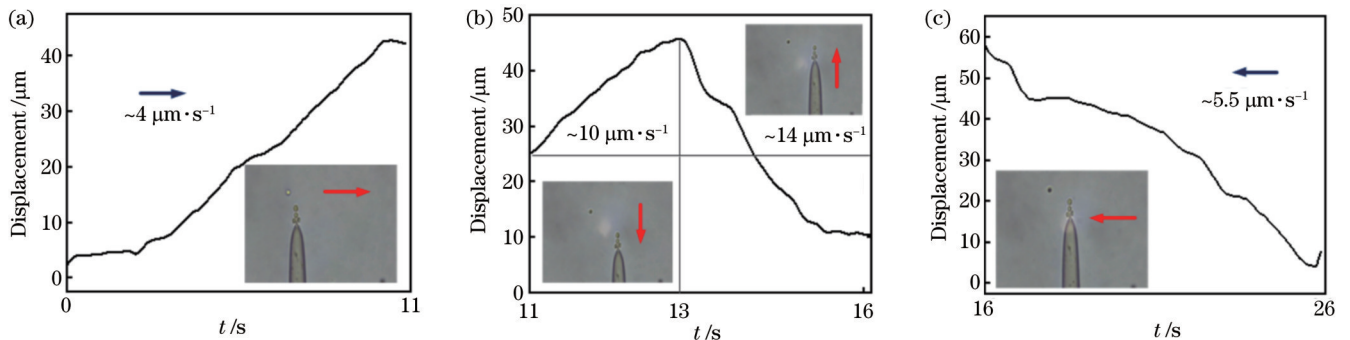

图 9 小球藻细胞随光纤运动的位移与时间关系图。(a)小球藻细胞随光纤向右运动;(b)小球藻细胞随光纤上下运动;(c)小球藻细胞随光纤向左运动

Fig. 9 Plots of displacement varying with time for motion of *Chlorella* cells with fiber. (a) *Chlorella* cells moving to right with fiber; (b) *Chlorella* cells moving up and down with fiber; (c) *Chlorella* cells moving to left with fiber

4 结 论

研究了一种用于多生物细胞多路排列的单光纤光镊。该光镊利用两种不同模式的光纤错位拼接,使输出光场中LP$_{01}$和LP$_{11}$模式共存,由于两种模式光束具有不同的传播常数,故表现出不同的聚焦光场,从而可以实现在不同方向捕获多个生物细胞。利用仿真模型,对 980 nm SMF 和 1550 nm SMF 复合的光纤光镊的光场分布进行了模拟,并分析了小球藻细胞的受力情况。实验表明,该光镊能够在三个方向对多个小球藻细胞进行同时捕获,并形成生物链条,在光纤移动速

度达到约为 14 μm/s 时仍能保持捕获稳定。该光纤光镊结构简单,为生物传感和直接检测生物信号提供了更多可能。

参 考 文 献

[1] Ashkin A, Dziedzic J M, Bjorkholm J E, et al. Observation of a single-beam gradient force optical trap for dielectric particles[J]. Optics Letters, 1986, 11(5): 288-290.

[2] Block S M, Goldstein L S B, Schnapp B J. Bead movement by single kinesin molecules studied with optical tweezers[J]. Nature, 1990, 348(6299): 348-352.

[3] Tskhovrebova L, Trinick J, Sleep J A, et al. Elasticity and unfolding of single molecules of the giant muscle protein titin[J].

Nature, 1997, 387(6630): 308-312.

[4] Wang M D, Yin H, Landick R, et al. Stretching DNA with optical tweezers[J]. Biophysical Journal, 1997, 72(3): 1335-1346.

[5] Chiou P Y, Ohta A T, Wu M C. Massively parallel manipulation of single cells and microparticles using optical images[J]. Nature, 2005, 436(7049): 370-372.

[6] Pang Y J, Song H N, Kim J H, et al. Optical trapping of individual human immunodeficiency viruses in culture fluid reveals heterogeneity with single-molecule resolution[J]. Nature Nanotechnology, 2014, 9(8): 624-630.

[7] Zhong M C, Wei X B, Zhou J H, et al. Trapping red blood cells in living animals using optical tweezers[J]. Nature Communications, 2013, 4: 1768.

[8] Liu R, Zheng L N, Matthews D L, et al. Power dependent oxygenation state transition of red blood cells in a single beam optical trap[J]. Applied Physics Letters, 2011, 99(4): 043702.

[9] Liu R, Mao Z L, Matthews D L, et al. Novel single-cell functional analysis of red blood cells using laser tweezers Raman spectroscopy: application for sickle cell disease[J]. Experimental Hematology, 2013, 41(7): 656-661.

[10] Garcés-Chávez V, McGloin D, Melville H, et al. Simultaneous micromanipulation in multiple planes using a self-reconstructing light beam[J]. Nature, 2002, 419(6903): 145-147.

[11] Padgett M, di Leonardo R. Holographic optical tweezers and their relevance to lab on chip devices[J]. Lab on a Chip, 2011, 11(7): 1196-1205.

[12] Grier D G. A revolution in optical manipulation[J]. Nature, 2003, 424(6950): 810-816.

[13] Dholakia K, Čižmár T. Shaping the future of manipulation[J]. Nature Photonics, 2011, 5(6): 335-342.

[14] Zhan Q W. Radiation forces on a dielectric sphere produced by highly focused cylindrical vector beams[J]. Journal of Optics A, 2003, 5(3): 229-232.

[15] Wang L G, Zhao C L, Wang L Q, et al. Effect of spatial coherence on radiation forces acting on a Rayleigh dielectric sphere[J]. Optics Letters, 2007, 32(11): 1393-1395.

[16] Zhao C L, Lu X H, Cai Y J. Radiation force of coherent and partially coherent flat-topped beams on a Rayleigh particle[J]. Optics Express, 2009, 17(3): 1753-1765.

[17] Zhao C L, Cai Y J. Trapping two types of particles using a focused partially coherent elegant Laguerre-Gaussian beam[J]. Optics Letters, 2011, 36(12): 2251-2253.

[18] 荣升, 刘洪双, 钟莹, 等. 基于光力捕获金纳米立方体的拉曼光谱增强[J]. 光学学报, 2021, 41(17): 1730003.
Rong S, Liu H S, Zhong Y, et al. Enhancement of Raman spectra based on optical trapping of gold nanocubes[J]. Acta Optica Sinica, 2021, 41(17): 1730003.

[19] 申泽, 成煜, 邓洪昌, 等. 鸟喙形环形芯光纤光镊粒子捕获受力分析[J]. 光学学报, 2021, 41(18): 1808001.
Shen Z, Cheng Y, Deng H C, et al. Analysis of trapping force of beak-shaped optical tweezers with annular core fibers for particles[J]. Acta Optica Sinica, 2021, 41(18): 1808001.

[20] 王驰, 温珠莉, 孙建美, 等. 基于超小自聚焦光纤探头的SS-OCT测振方法研究[J]. 光学学报, 2021, 41(15): 1511002.

Wang C, Wen Z L, Sun J M, et al. Research on SS-OCT vibration measurement method based on ultra-small GRIN fiber probe[J]. Acta Optica Sinica, 2021, 41(15): 1511002.

[21] 吴健华, 张晓锋, 陈亮, 等. 全光纤微电流传感器研究进展[J]. 激光与光电子学进展, 2022, 59(17): 1700005.
Wu J H, Zhang X F, Chen L, et al. Research progress of all-fiber optic micro-current sensor[J]. Laser & Optoelectronics Progress, 2022, 59(17): 1700005.

[22] Liu Y X, Yu M. Multiple traps created with an inclined dual-fiber system[J]. Optics Express, 2009, 17(24): 21680-21690.

[23] Barron A L, Kar A K, Aspray T J, et al. Two dimensional interferometric optical trapping of multiple particles and Escherichia coli bacterial cells using a lensed multicore fiber[J]. Optics Express, 2013, 21(11): 13199-13207.

[24] Xin H B, Xu R, Li B J. Optical formation and manipulation of particle and cell patterns using a tapered optical fiber[J]. Laser & Photonics Reviews, 2013, 7(5): 801-809.

[25] Lei H X, Zhang Y, Xu C, et al. Photophoretic assembly of two-dimensional crystals from microparticle suspensions[J]. Journal of Optics, 2012, 14(3): 035603.

[26] Li Y C, Liu X S, Yang X G, et al. Enhancing upconversion fluorescence with a natural bio-microlens[J]. ACS Nano, 2017, 11(11): 10672-10680.

[27] Xin H B, Li Y C, Li B J. Controllable patterning of different cells via optical assembly of 1D periodic cell structures[J]. Advanced Functional Materials, 2015, 25(19): 2816-2823.

[28] Liu X S, Huang J B, Li Y C, et al. Rotation and deformation of human red blood cells with light from tapered fiber probes[J]. Nanophotonics, 2017, 6(1): 309-316.

[29] Velázquez-Benítez A M, Guerra-Santillán K Y, Caudillo-Viurquez R, et al. Optical trapping and micromanipulation with a photonic lantern-mode multiplexer[J]. Optics Letters, 2018, 43(6): 1303-1306.

[30] Zhang Y, Liang P B, Lei J J, et al. Multi-dimensional manipulation of yeast cells using a LP_{11} mode beam[J]. Journal of Lightwave Technology, 2014, 32(6): 1098-1103. [LinkOut]

[31] Liu Z H, Wang L, Liang P B, et al. Mode division multiplexing technology for single-fiber optical trapping axial-position adjustment[J]. Optics Letters, 2013, 38(14): 2617-2620.

[32] Zhang Y X, Zhou Y, Tang X Y, et al. Mode division multiplexing for multiple particles noncontact simultaneous trap[J]. Optics Letters, 2021, 46(13): 3017-3020.

[33] Zhang Y X, Wang C, Zhang Y, et al. Single fiber optical tweezer for particles multi-dimensional arrangement[J]. Journal of Lightwave Technology, 2022, 40(4): 1144-1149.

[34] Aas E. Refractive index of phytoplankton derived from its metabolite composition[J]. Journal of Plankton Research, 1996, 18(12): 2223-2249.

[35] Schmidt B S, Yang A H, Erickson D, et al. Optofluidic trapping and transport on solid core waveguides within a microfluidic device[J]. Optics Express, 2007, 15(22): 14322-14334.

[36] Li Y C, Xin H B, Cheng C, et al. Optical separation and controllable delivery of cells from particle and cell mixture[J]. Nanophotonics, 2015, 4(3): 353-360.

Single-Fiber Optical Tweezer Based on Coexistence of LP$_{01}$ and LP$_{11}$ Modes for Multiplexed Capture and Manipulation of Biological Cells

Chen Peng, Dang Yuting, Zhong Hui, Jiang Chunlei[*]

College of Electrical and Information Engineering, Northeast Petroleum University, Daqing 163318, Heilongjiang, China

Abstract

Objective　　Currently, some biophotonic devices or cell-to-cell interactions and communications require the capture of particles, especially multiple particles. Since the invention of optical tweezers in 1986, optical tweezers have become an important tool that is widely used in the manipulation and study of cells, viruses, atoms, colloids, and other particles. Based on conventional optical tweezers, multi-directional alignment of multiple particles is achieved by various methods such as holographic optical tweezers, single beam before helical phase, and optical binding. However, these techniques require bulky optical components, which complicates optical tweezer systems and hinders operational flexibility. To overcome the shortcomings of conventional optical tweezers in capturing multiple particles, researchers have used optical tweezers to capture multiple particles. Some researchers have created multiple optical traps using dual fibers, which enables the capture of multiple particles in two and three dimensions, and they have manipulated, deflected, and stretched multiple cells using two misaligned single-mode fibers. Some researchers have used multicore fibers for two-dimensional optical interference capture of multiple particles and *Escherichila coli* cells manipulation of multiple particles using photonic crystal mode multiplexing, while others have used fiber traps and photothermal effects to manipulate a large number of particles. However, the optical fiber probes in the above methods with multi-core fibers and photonic crystals are, in general, structurally complex, and difficult to replicate. Focusing on the complex structure of multi-core fiber and photonic crystal fiber probe, this paper proposes a single-fiber optical tweezer structure with two modes being composite. The structure utilizes two different modes of fiber staggered splicing to ensure the LP$_{01}$ and LP$_{11}$ modes coexist in the output optical field, and the two modes of the beam have different focused optical fields to achieve the capture of multiple *Chlorella* cells in different directions. The captured *Chlorella* cells act as lenses to refocus the beam to capture the next cell and then form multiple biological chains.

Methods　　In order to make LP$_{01}$ and LP$_{11}$ mode beams coexist in the fiber, 980 nm single mode fiber (SMF) and 1550 nm SMF are utilized for splicing (Fig. 1). The energy ratio of the LP$_{01}$ and LP$_{11}$ mode beams is also controlled by controlling the offset of the two fiber splices, which in turn ensures that each optical trap can have sufficient optical power to trap particles. In order to analyze the focused optical field characteristics of the composite mode fiber, a two-dimensional model based on finite element analysis is developed using simulation software. The output optical field distribution of the composite fiber with 980 nm SMF and 1550 nm SMF staggered by 2 μm is simulated, and the optical radiation pressure applied to *Chlorella* cells is calculated. The simulation results show that the LP$_{01}$ mode beam is focused at the tip of the fiber probe and forms an optical potential well [Fig. 4 (a)]. The LP$_{11}$ mode has a completely different light field at the tip of the fiber probe [Fig. 4 (b)]. The LP$_{11}$ mode light field is not concentrated near the optical axis. The convergence position of the LP$_{11}$ mode beam is inside the fiber tip. Due to the special fiber shape, the light field gradient distribution on the side of the fiber is large, so *Chlorella* cells outside the fiber tip will be attracted and move toward the fiber tip and eventually be captured. The coexistence of the LP$_{01}$ and LP$_{11}$ mode beams integrates the characteristics of both LP$_{01}$ and LP$_{11}$ mode beams [Fig. 4 (c)]. The LP$_{01}$ mode beam is also present while the LP$_{11}$ mode beam is excited in the fiber, and the two-mode beams exhibit different focused light fields because they have different propagation constants. In other words, the LP$_{01}$ and LP$_{11}$ modes produce different stable capture points when passing through the same fiber probe. When LP$_{01}$ and LP$_{11}$ modes coexist, the simulation results show that *Chlorella* cells are captured on both sides of the optical axis and the fiber tip, respectively (Fig. 5).

Results and Discussions　　To verify the validity of the simulation analysis, we build an experimental setup (Fig. 6) and conduct experiments on the capture and capture stability of *Chlorella* cells by using optical tweezers. The 980 nm SMF is connected to a laser source with a wavelength of 980 nm as the input, and the 1550 nm SMF is immersed in the *Chlorella* cell solution as the output. When the laser is turned on, the *Chlorella* cells in the effective trap area of the optical fiber probe are attracted to the fiber tip. Due to the stronger light field gradient distribution on both sides of the fiber tip, the *Chlorella* cells are trapped on both sides of the fiber tip (Fig. 7). The experimental results show that the optical tweezer structure is able to simultaneously trap multiple *Chlorella* cells in three directions and form a biological chain. The capture

remains stable when the fiber moves at a speed of about 14 μm/s (Fig. 9).

Conclusions　　In summary, a single-fiber optical tweezer for multiplexed alignment of multi-biological cells is proposed in this paper. The optical tweezer utilizes two different modes of fiber staggered splicing to make LP_{01} and LP_{11} modes coexist in the output optical field. Since the two mode beams have different propagation constants and exhibit different focused light fields, the capture of multi-biological cells in different directions can be achieved. Through the finite element analysis method, the optical field distribution of the optical fiber tweezer with 980 nm SMF and 1550 nm SMF being composite is simulated, and the force on *Chlorella* cells is analyzed. Finally, it is shown that the optical tweezer can capture multiple *Chlorella* cells simultaneously in three directions and form a biological chain. The capture remains stable when the fiber travels at a speed of about 14 μm/s. The simple structure of this optical fiber tweezer provides more possibilities for biosensing and direct detection of biosignals.

Key words　　fiber optics; fiber optical tweezers; LP_{01} mode and LP_{11} mode; multiplexed capture and manipulation; biosensing